Journal of Applied Physics

RESEARCH ARTICLE | NOVEMBER 11 2022

Crystal side facet-tuning of GaN nanowires and nanofins grown by molecular beam epitaxy

Florian Pantle ; Monika Karlinger; Simon Wörle ; Fabian Becker ; Theresa Höldrich; Elise Sirotti; Max Kraut ; Martin Stutzmann

J. Appl. Phys. 132, 184304 (2022)
https://doi.org/10.1063/5.0098016

AIP Publishing

Journal of Applied Physics ARTICLE scitation.org/journal/jap

Crystal side facet-tuning of GaN nanowires and nanofins grown by molecular beam epitaxy

Cite as: J. Appl. Phys. **132**, 184304 (2022); doi: 10.1063/5.0098016
Submitted: 4 May 2022 · Accepted: 22 October 2022 ·
Published Online: 11 November 2022

Florian Pantle,[a] Monika Karlinger, Simon Wörle, Fabian Becker, Theresa Höldrich, Elise Sirotti, Max Kraut, and Martin Stutzmann[b]

AFFILIATIONS

Walter Schottky Institut and Physics Department, Technische Universität München, Am Coulombwall 4, 85748 Garching, Germany

[a]**Author to whom correspondence should be addressed:** florian.pantle@wsi.tum.de
[b]**Electronic mail:** stutz@wsi.tum.de

ABSTRACT

GaN nanostructures are promising for a broad range of applications due to their 3D structure, thereby exposing non-polar crystal surfaces. The nature of the exposed crystal facets, i.e., whether they are a-, m-plane, or of mixed orientation, impacts the stability and performance of GaN nanostructure-based devices. In this context, it is of great interest to control the formation of well-defined side facets. Here, we show that we can control the crystal facet formation at the nanowire sidewalls by tuning the III–V ratio during selective area growth by molecular beam epitaxy. Especially, the N flux serves as a tool for controlling the growth kinetics. In addition, we demonstrate the growth of GaN nanofins with either a- or m-plane side facets. Based on our observations, we present the underlying nanostructure growth mechanisms. Low temperature photoluminescence measurements show a correlation of the formation of structural defects like stacking faults with the growth kinetics. This article demonstrates the controlled selective epitaxy of GaN nanostructures with defined crystal side facets on large-scale available AlN substrates.

I. INTRODUCTION

The areas of application of group III-nitride nanostructures (NSs) range from optoelectronics[1–7] and high-power electronics[8–13] to photo-catalysis[14–16] and sensing devices.[17–20] In particular, for the latter two applications, control over the nature of the side facets is essential. For instance, it is known that the m- and a-plane exhibit a different stability under illumination in aqueous environments.[21] The most prominent NS representatives are GaN nanorods and nanowires (NWs), typically exposing mixed non-polar facets with a tendency toward the m-plane. Lately, it has been shown that self-assembled GaN nanowires develop m-plane side facets at their upper part while acquiring roundish cross-sectional shapes at their bottom due to annealing and shadowing effects.[22] For GaN nanofins (NFs), their growth with stable a- and m-plane facets is possible by predetermining their lateral alignment with the crystal orientation of the substrate.[23] However, reports about the intentional growth of a-plane NWs are scarce. In the literature, the appearance of a-plane side facets is observed in early nucleation stages of non-vapor liquid solid (VLS) grown dodecagonal NWs, which evolve toward stable hexagonal m-plane GaN NWs during the further growth process.[24] Recently, GaN microrods with stable a-plane side facets were reported, where the stabilization of the a-plane facets was induced by adding arsenic during VLS-growth.[25]

In this study, we present the controlled growth of GaN NWs and NFs on AlN templates. By tuning the III-V ratio during the non-VLS plasma-assisted molecular beam epitaxy (MBE), we are able to tune the nature of the exposed non-polar side facets. In this context, we discuss the morphology of GaN NFs with a- and m-plane side facets. NFs gain increasing interest as electrical contacts are easier to achieve, which enables the possibility of lateral devices like, e.g., sensors or fin field-effect transistors (FinFETs). Based on our observations, we propose a model for the growth mechanism. Structural and electronic characterization was performed by means of low temperature photoluminescence (PL) measurements of the NSs.

II. EXPERIMENTAL

Group III-nitride NSs were grown on 2.1 μm thick Al-polar AlN templates on double-side polished c-plane sapphire with a size of $10 \times 10\,\text{mm}^2$ purchased from Xiamen Powerway Advanced Material Co., Ltd. The AlN epitaxial layer ensures Ga-polarity of the selective NSs in contrast to the growth on, e.g., sapphire where they would nucleate with a mixed polarity.[26] The AlN substrates are characterized by a smooth surface (step flow growth with terraces of atomic height) with a root mean square roughness of approx. 0.3 nm and a high crystal quality with a 2θ full width at half maximum (FWHM) of the (0002) reflex of 0.03° and a ω-rocking curve FWHM of 0.014°. The corresponding x-ray diffraction (XRD) data and atomic force microscopy (AFM) images of the AlN surface are provided in the supplementary material.

The substrate back sides were coated with 200 nm Ti followed by 70 nm Pt in order to enhance the heat absorption from the radiative heater during MBE growth. Thus, the substrate temperatures quoted in this article refer to thermocouple values of the substrate heater, which overestimates the real temperatures at the AlN surface.

The GaN NSs investigated in this work were grown in a custom-made Tectra "Mini-MBE" purchased from Dr. Eberl MBE-Komponenten GmbH in a selective area growth mode. To this end, 10 nm of Ti were evaporated onto the sample surface as a mask material. The Ti mask was patterned via electron beam lithography with arrays of holes and lines, which serve as nucleation spots for the NW and NF growth, respectively. Prior to the MBE growth, the substrates were etched with hydrochloric acid in order to remove the native surface oxide and to gain a reproducible surface termination. The MBE growth started with a nitridation of the samples by exposure to a nitrogen plasma with a flux of 0.36 SCCM and an RF plasma power of 425 W at 400 °C and 800 °C for 10 and 5 min, respectively. This leads to the conversion of the Ti mask into a more stable TiN_x layer. The actual GaN NS growth was performed with different N fluxes as denoted in the text but a constant plasma power of 425 W. If not otherwise mentioned, a Ga flux of 0.6×10^{-6} mbar beam equivalent pressure (BEP) was chosen and the substrate temperature was set to 960 °C during the growth time of 90 min. A detailed description of the NS fabrication process can be found in previous publications.[23,27,28] The background pressure of the MBE system was in the 10^{-10} mbar range.

(High resolution) XRD measurements were performed with a Rigaku SmartLab x-ray diffractometer using a Cu cathode operating at 40 kV. A Ge double-bounce monochromator to select the $Cu_{K\alpha 1}$ emission line ($\lambda = 1.540\,59$ Å) and a HyPix3000 CCD detector in the point (0 D) mode were used for the high resolution XRD measurements of the AlN substrates. ϕ-scans were carried out without monochromator. The in-plane epitaxy and, thereby, the assignment of the sidewalls to a certain non-polar facet (either a- or m-plane) was determined in combination with SEM images (Fig. 1): We observe a sixfold symmetry for the AlN substrate and the GaN NW array. The in-plane orientation of the GaN nanostructures follows the orientation of the substrate. Note that the XRD peaks of the AlN and GaN are sufficiently sharp and separated from each other as discussed in the supplementary material. The right part of Fig. 1 depicts a top view SEM image of the GaN NWs and the direction of the incident x-ray beam for $\phi = 0°$. As we observe the XRD peaks of the ($\bar{1}103$) wurtzite reflexes at angles of $\phi = 30°, 90°, \ldots$, the depicted NWs exhibit a-plane side facets, which is illustrated by the blue hexagon.

For the above-bandgap excitation of the GaN NSs during the PL measurements, a quadrupled Nd:YAG laser with a wavelength of 266 nm in a continuous wave operation was used. A convergent lens with a focal length of 70 mm guided the light into an Oxford Instruments He flow cryostat, which resulted in a spot size of

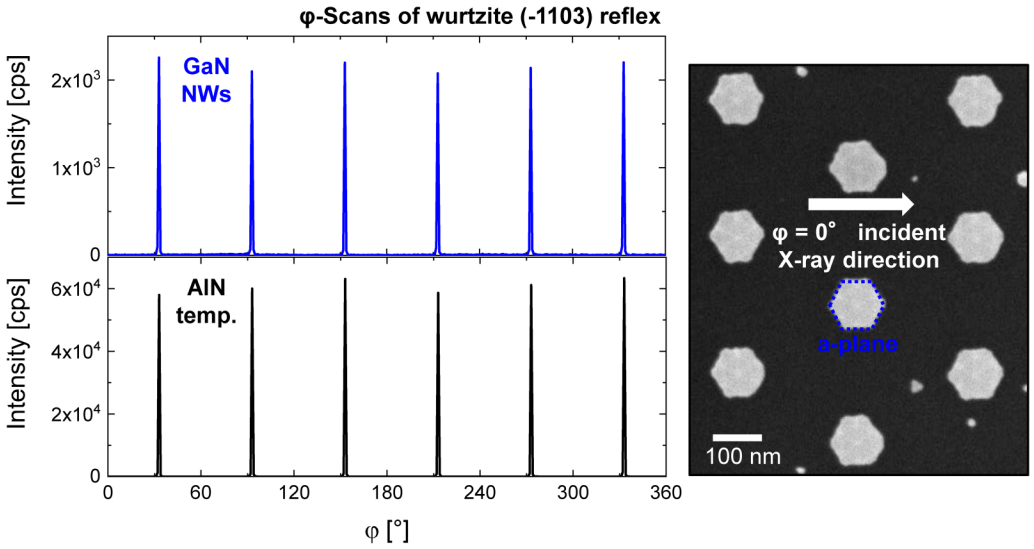

FIG. 1. XRD pole figures of GaN NWs (blue) and the AlN substrate (black) measured at the wurtzite ($\bar{1}103$) reflex. The top view SEM image shows the measured NWs and the direction of the incident x-ray beam for $\phi = 0°$.

approx. 50 μm on the sample surface. The excitation power was set to 0.13 W/cm^2. The PL signal passed a DILOR double spectrometer with a focal length of 800 mm and was detected by a Peltier-cooled photo-multiplier tube with a dark count rate of 15 counts per second (cps).

III. RESULTS AND DISCUSSION

In order to study the influence of the growth conditions on the morphology of GaN NSs, the Ga flux, the N flux, and the growth duration were varied. Comparative PL measurements were carried out on NSs grown with the lowest and highest N flux, respectively.

A. Nitrogen flux series

Scanning electron microscopy (SEM) images of GaN NWs in dependence on the N flux are depicted in Fig. 2. Furthermore, the nominal NW diameter, which is controlled by the size of the hole in the Ti mask, is increased from the left to the right. In the 45°-tilted view images [Fig. 2(a)], it can be seen that the NW height increases from approx. 200 nm to over 500 nm for higher N fluxes independent of the NW thickness. The almost linear dependence of the axial and lateral growth rates [cf. Figs. 4(a) and 4(b)] shows that the growth was conducted in the N-limited regime. The morphology of the NWs depends on the N flux, which becomes apparent in the top view SEM images shown in Fig. 2(b). At low N fluxes and small diameters, hexagonal NWs with sharp edges and m-plane $\{1\bar{1}00\}$ side facets (indicated by red hexagons in this article) are formed. In contrast, for thick NWs and at high N fluxes, we obtained a-plane $\{11\bar{2}0\}$ (green hexagons) NWs with more blunt edges and slightly curved side facets. In the intermediate regime of medium thick NWs and moderate N fluxes, we observe round or polygonal NWs with a tendency to be a-plane alike. In particular, for the lowest N flux of 0.18 SCCM, it is possible to switch from m- to a-plane NWs by only increasing their nominal diameter.

All NWs have a tapered top exposing semi-polar crystal facets of the $\{1\bar{1}0n\}$-family. Consequently, the top facet cut lines [orange lines in Fig. 2(b)] of the a-plane NWs point toward the middle of their side facets while for the m-plane NWs, these cut lines point into the NW edges, which is in accordance to other hexagonal m-plane GaN NWs in the literature.[24,29] While we determined the $\{1\bar{1}02\}$ planes being the top facets of the m- and a-plane NWs grown at low N fluxes [Figs. 3(a) and 3(b)], an assignment to a certain family of $\{1\bar{1}0n\}$ planes was more difficult for the a-plane NWs grown at high N fluxes due to their rounded NW tops. Nevertheless, at the outside of these NWs we also determined n = 2. Note that the inter-NS distance has no influence on the selectivity of the NS growth (not shown).

B. Gallium flux series

To further understand the influence of the III-V ratio during MBE growth on the GaN NW side facets, a Ga flux series was performed with a constant intermediate N flux of 0.36 SCCM. Figure 5 shows SEM images of GaN NWs (left) as well as m- and a-plane NFs (right) grown with an increasing Ga flux. An analysis of the

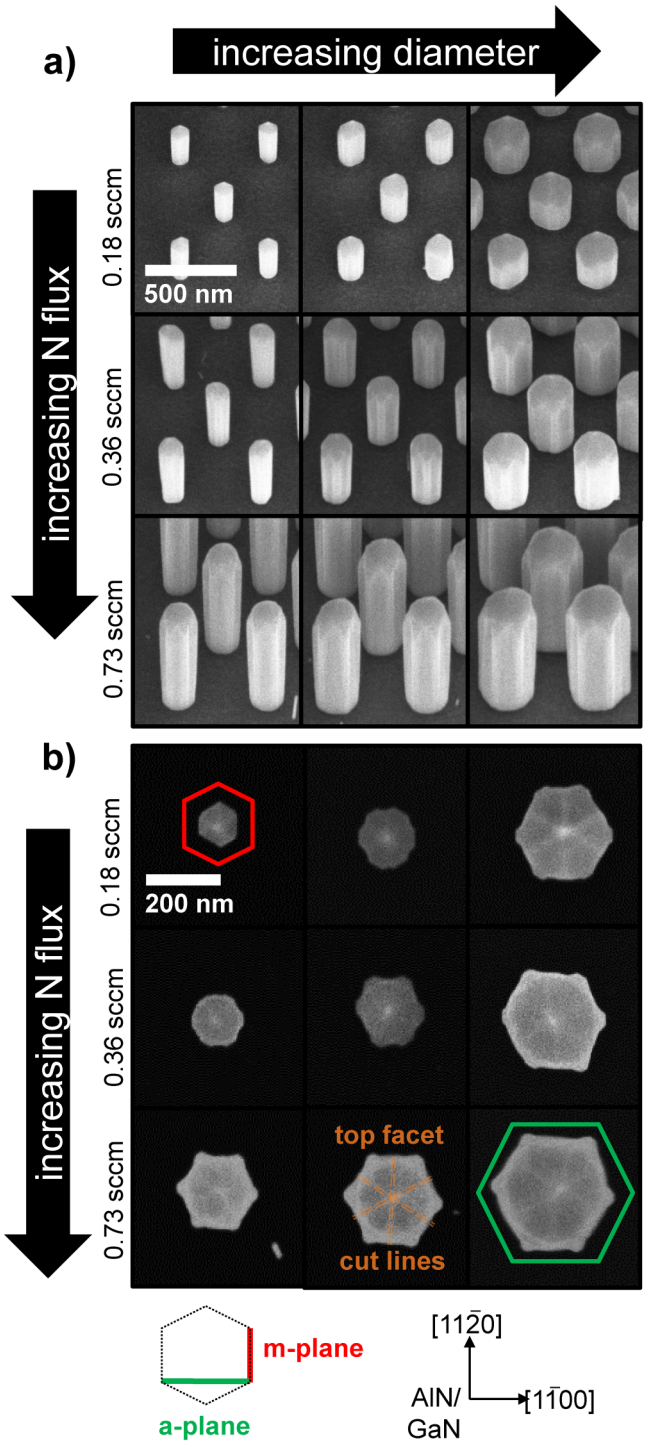

FIG. 2. SEM images in (a) 45°-tilted view and (b) top view of GaN NWs grown at N fluxes of 0.18, 0.36, and 0.73 SCCM on AlN/sapphire templates. Their nominal diameter is varied from the left to the right. The red (green) hexagons mark the orientation of the wurtzite m-(a-) plane.

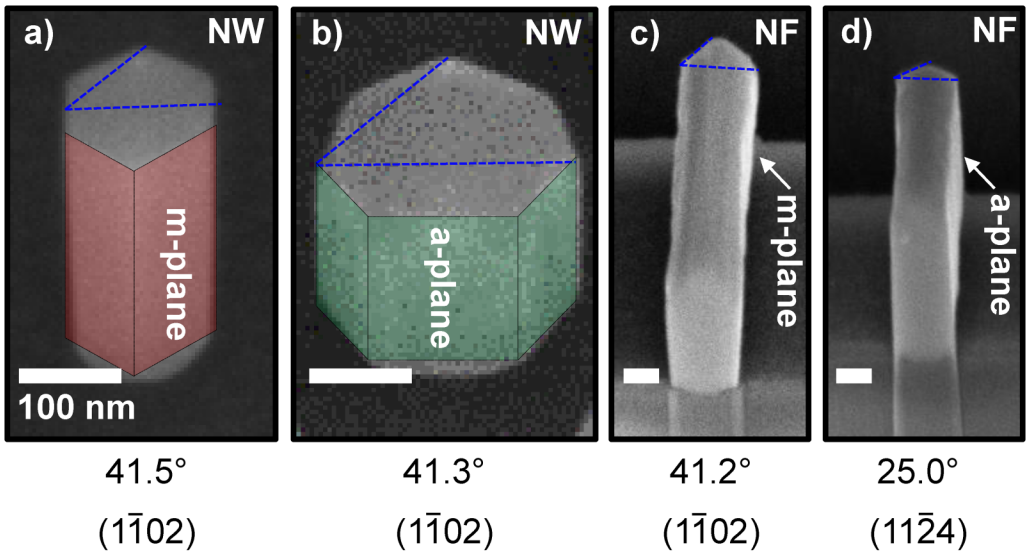

FIG. 3. 45°-tilted view SEM images of (a) an m-plane NW, (b) an a-plane NW, (c) an m-plane NF, and (d) an a-plane NF. The blue lines indicate the top facet tapering angles, which are noted below together with the assigned Miller indices. The depicted NFs were cut out of longer fins by means of a focused Ga ion beam in order to make their top facets visible in the tilted SEM image.

NW dimensions yields a strong dependence of the NW height for Ga fluxes below approx. 0.6×10^{-6} mbar BEP [Fig. 4(c)]. There, the growth switches into the Ga-limited regime. Most important, m-plane NW side facets have been observed for the lowest and highest Ga fluxes used. Note that the shape of the nanorods grown at very low Ga fluxes is rather distorted, while we obtained typical hexagonal-shaped NWs at high Ga fluxes. In the intermediate Ga flux regime, no clearly defined side facets evolved. Nevertheless, these NWs tend to be rather a- than m-plane.

In the right part of Fig. 5, SEM images of GaN NFs are shown. The fins either expose the a- or the m-planes as side facets, depending on their epitaxial orientation relative to the substrate.[23]

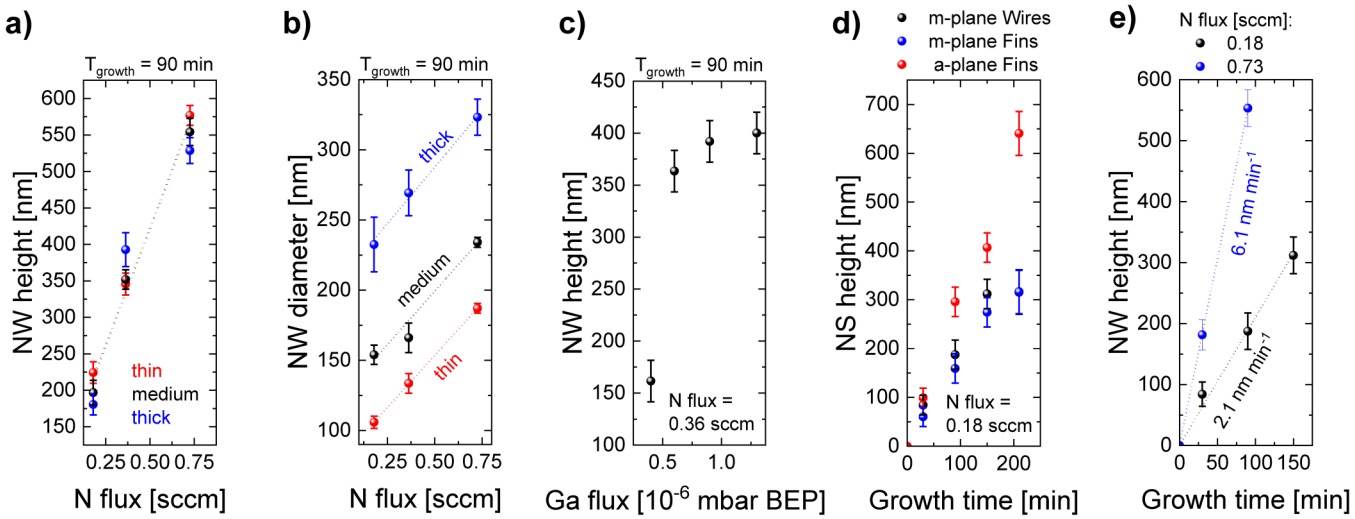

FIG. 4. Evaluation of the NS dimensions determined by SEM images: (a)/(b) heights/diameters of thin (medium, thick) NWs in dependence on the N flux in red (black, blue). (c) NW height in dependence on the Ga flux. (d) NS height after a certain growth duration for m-plane NWs (m-plane NFs, a-plane NFs) in black (blue, red). (e) growth rates for a low and high N flux, respectively. Except for (c), the Ga flux was fixed to 0.6×10^{-6} mbar BEP.

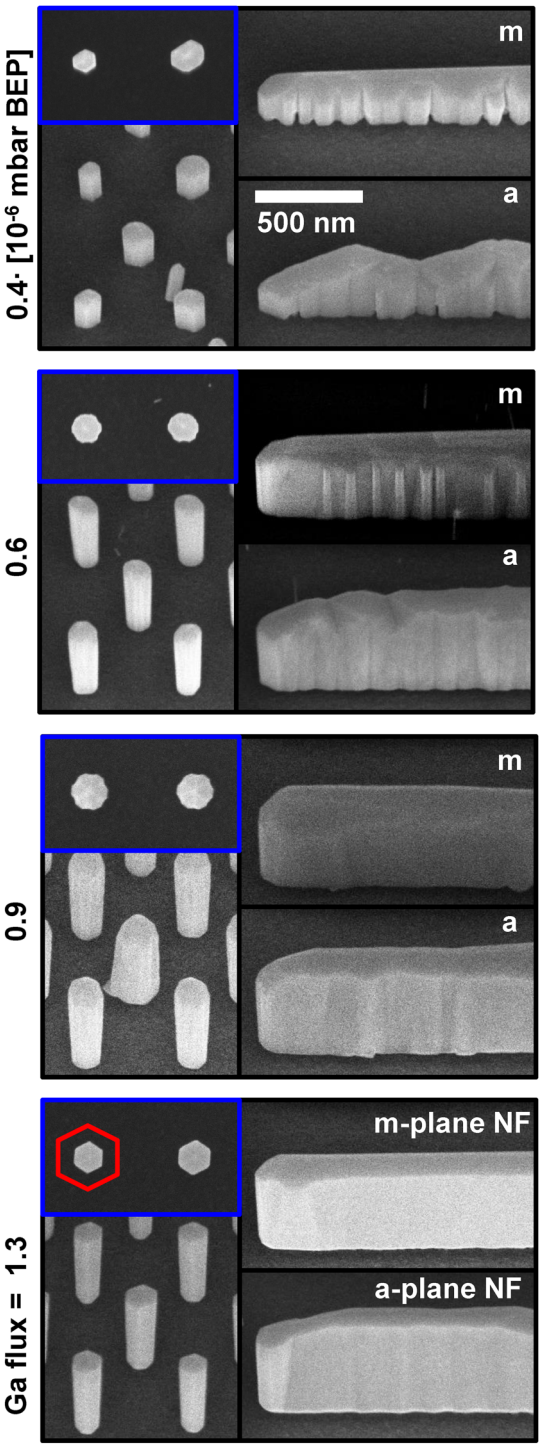

FIG. 5. Top view (blue-framed) and 45°-tilted view (black-framed) SEM images of GaN NWs (left) as well as m- and a-plane NFs (right) for an increasing Ga flux from 0.4 to 1.3 × 10^{-6} mbar BEP (from top to bottom). The N flux was fixed at 0.36 SCCM.

We observe a strong smoothing of the NF side facets for an increased Ga supply. The height of the NFs also increases for higher Ga fluxes. Especially for the larger NFs, two distinct differences between the two NF types can be observed: (1) the end parts of m- and a-plane NFs differ. While the m-plane NFs retain their height almost until the end of the fin, there is a shoulder observable at the end of the a-plane NFs. (2) a- and m-plane NFs exhibit different top facet angles, which can be better seen in the side-view images in Figs. 3(c) and 3(d). The m-plane NFs expose $\{1\bar{1}02\}$ top facets alike the NWs, while the a-plane fins have flatter $\{11\bar{2}4\}$ planes at the top.

C. Influence of growth duration

In order to understand the underlying mechanism of the NS formation, their morphology evolution during MBE growth is of interest. To address this issue, SEM images of GaN NSs after certain growth times have been recorded. Figure 6(a) shows the evolution of GaN NSs grown at a N flux of 0.18 SCCM for a growth duration of 30 min up to 210 min. In the top view images it can be seen that the thin NWs develop their hexagonal m-plane shape already after 30 min. The thick NWs are not yet uniformly shaped after 30 min growth. In contrast, the typical shapes of the a- and m-plane NFs discussed above already occur in this early stage. When the growth time is increased to 90 min, the thin NWs maintain their morphology and after 210 min we end up with clearly faceted wires. In contrast, the thick NWs evolve to a-plane NWs after 90 min and end up with a mixed amount of a- and m-plane side facets after 210 min. The overall morphology of the NFs does not change after 210 min. However, it can be seen that the side facets of the a-plane NFs are significantly higher than these of the m-plane NFs and of the NWs [approx. 600 nm instead of 300 nm, cf. Fig. 4(d)]. Interestingly, the end of the a-plane NF shoulder has the same height as the NWs [indicated by the orange lines in Fig. 6(a)]. Note that the lateral extension of this shoulder also increases with increasing growth duration.

When the N flux is increased to 0.72 SCCM [Fig. 6(b)], a-plane NWs with slightly washed out side facets evolve already after 30 min, independent of their nominal diameter, and stay in their a-plane shape for a growth duration up to 90 min (cf. Fig. 2). A significantly longer growth duration was not accessible as the selectivity of the process gets lost for longer growth times due to a degradation of the Ti mask at these high N fluxes where parasitic NWs would dominate the sample as a consequence. From the variation of the growth duration, we were able to assess the axial growth rate at the low N flux of 0.18 SCCM to approx. 2 nm/min. At a high N flux of 0.73 SCCM, we estimate approx. 6 nm/min [Fig. 4(e)].

D. Nanostructure formation mechanisms

Our proposed growth model is based on the following observations: (1) in the N-limited regime, the axial growth rate always remains constant for a given Ga/N flux, regardless of the NW width, as shown in Fig. 4(a). The NW growth in the axial direction is favored over the lateral growth, which is the basic requirement for growing NWs with an aspect ratio >1. Further, the NWs grown at the "standard" Ga flux of 0.6 × 10^{-6} mbar BEP are synthesized

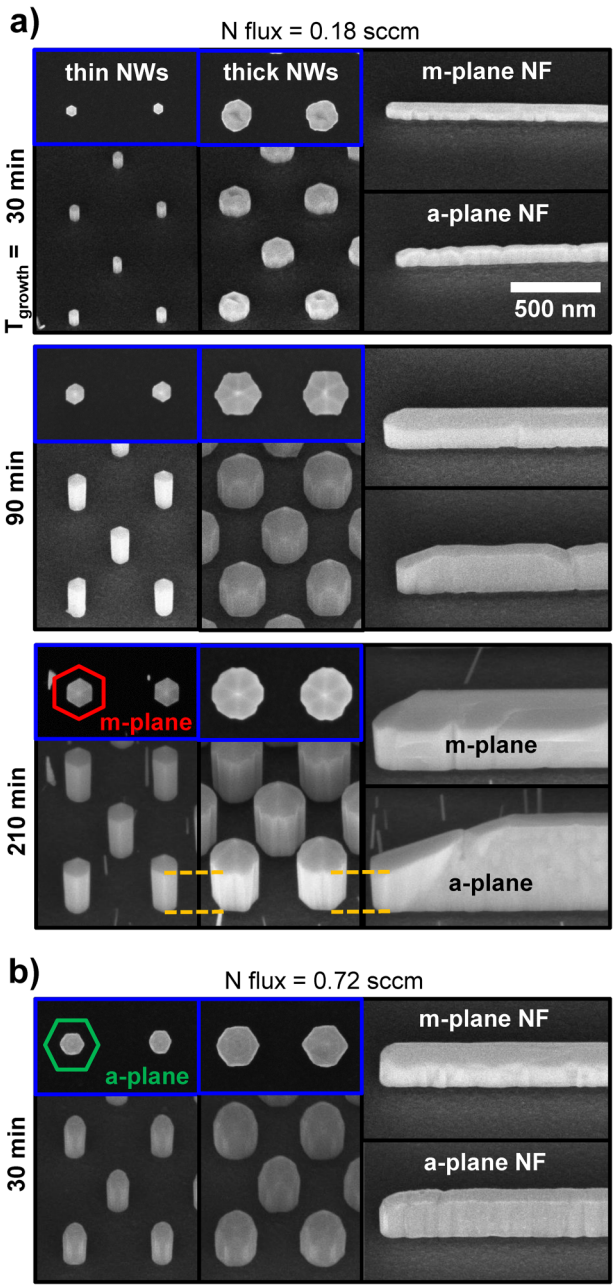

FIG. 6. Top view (blue-framed) and 45°-tilted view (black-framed) SEM images of GaN NSs after different growth times. The red and green hexagons mark the orientation of the m- and a-plane, respectively. (a) N flux = 0.18 SCCM. The dash orange lines serve as guide for the eye in order to compare the NS heights. (b) N flux = 0.72 SCCM.

at the limit to the Ga-limited regime. Accordingly, most of the available Ga atoms are consumed for the axial NW growth. (2) We suppose that the total Ga supply for each NW is linked to the NW diameter as follows: besides the directly impinging Ga atoms, the NWs collect Ga from the TiN_x mask within the Ga diffusion length, which is roughly 500 nm.[27] This value should roughly apply also to our samples, as the referenced study was performed in-house with the same type of mask material in the same MBE system with comparable growth parameters. In the case of thin NWs, the total Ga collection area relative to the NW cross-sectional area is larger than in the case of thick NWs (a calculation example is discussed in the supplementary material). This means that the total amount of available Ga relative to the NW cross-sectional area decreases for increasing NW diameters. Based on this, we explain the change in the NW morphology depending on the N flux as illustrated in Fig. 7(a): In the presented N-limited regime, the NW height strongly depends on the N flux. For thin NWs at low N fluxes [Fig. 7(a), left], an m-plane hexagonal shape evolves as the m-plane is energetically favorable over the a-plane (surface energy 124 and 132 meV/Å^2, respectively[30]) and the hexagonal cross section provides the lowest purely m-plane surface area. In the case of thick NWs grown under the same conditions, a larger 3D volume growth rate is needed to maintain the same axial (2D) growth rate compared to the thin NWs. Due to the lack of Ga atoms available for the thick NWs, these might initially form a star-like cross section [Fig. 7(a), right] as this enables the presence of mainly m-plane facets while lowering the volume per unit NW length, i.e., the NW is able to maintain its axial growth rate by lowering its volume growth due to a reduced star-like footprint compared to a hexagon. In the literature, comparable star-like GaN NWs grown by metal organic vapor phase epitaxy have been reported. There, a constant axial growth rate arose from a SiN passivation at the NW sidewalls during growth.[31] However, during the ongoing NW growth, impinging atoms and especially Ga from the mask within the collection area might be used to fill up the gaps between the star-tips, thereby forming a-plane facets after 90 min MBE growth [Fig. 6(a)]. Nevertheless, as the a-plane is energetically not favorable, we can observe that polygonal NWs with mixed a- and m-planes evolve after a longer growth duration of 210 min. The oddly shaped thick nanorods observed after the first 30 min are rather a consequence of the nucleation mechanism in the Ti mask hole where the morphology is characterized by the coalescence of various GaN nuclei,[24] which is expected to take longer for thicker NWs/larger mask holes.

It is known from the literature that the axial growth rate and the diameter of spontaneously formed GaN NWs are self-regulated. This means that in a steady-state regime, the final NW dimensions only depend on the III/V flux ratio during MBE growth.[32] However, in our study, the NSs might grow far from this mentioned steady-state equilibrium, especially in the N-rich regime. Thus, the morphology of our selectively grown NWs might be not subject to the mentioned self-regulatory mechanism.

When the NWs are grown under more N-rich conditions, their total height increases. Accordingly, the Ga atoms needed for the increased axial growth speed lack for forming an m-plane hexagonal footprint, even for the thinnest NWs. During the ongoing growth process, the m-plane star-like cross section evolves to a nearly a-plane hexagon, which is expected to happen shortly thereafter, as already after 30 min a-plane NWs have evolved at high N fluxes. This might lead to a morphology as depicted in Fig. 7(b), where a more star-like NW top and a more hexagonal bottom can

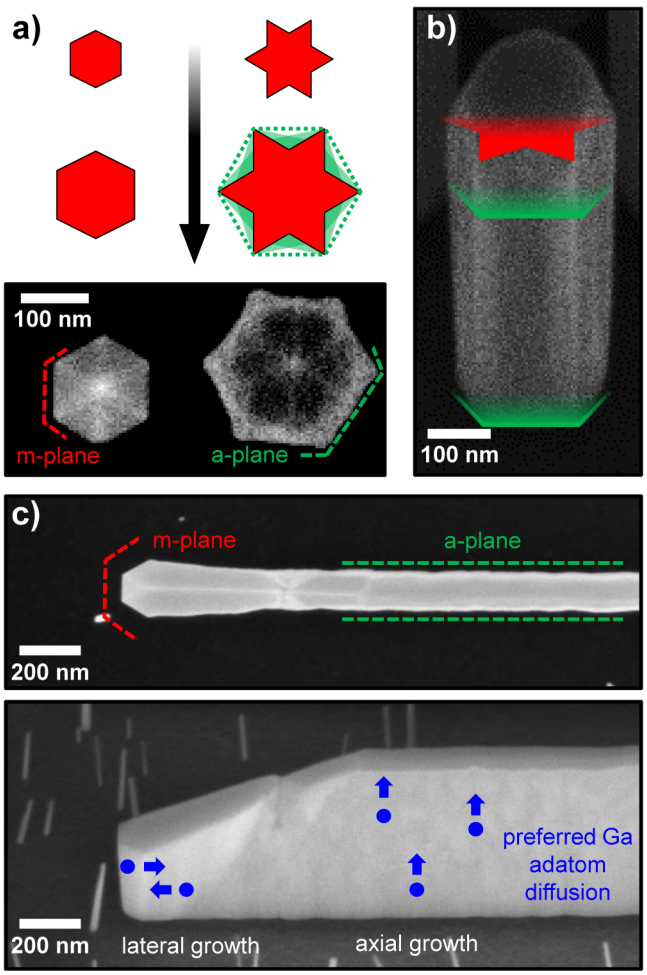

FIG. 7. Schematic image of the proposed growth mechanism. (a) Cross-sectional evolution of m- and a-plane NWs (left and right). (b) Close-up of a GaN NW grown at a high N flux of 0.72 SCCM after 90 min. The red star and the green hexagon indicate the origin of the NW formation mechanism. (c) NF grown at a low N flux of 0.18 sccm after 210 min. In the top view image (top), the green lines indicate the a-plane side facets and the red marks illustrate the m-plane end facets. The blue arrows in the 45°-tilted view picture (below) show the preferred Ga diffusion direction on both non-polar facets.

be seen on an SEM image of a NW. Further, the not completely straight but rather slightly inward bent a-plane side facets would be a consequence of the proposed growth model.

The Ga flux series confirms this hypothesis. For very high Ga fluxes above approx. 1.3×10^{-6} mbar BEP (Fig. 5, bottom image), the Ga supply is sufficient for building hexagonal m-plane cross sections. In contrast, at the lowest applied Ga flux of 0.4×10^{-6} mbar BEP, the axial growth is not limited by the N flux, but by the Ga supply. As a consequence, the axial growth rate is significantly reduced and, thereby, the volume growth rate needed to maintain a hexagonal m-plane cross section. In this Ga-limited regime, Ga from the Ti mask around the NW mainly contributes to a pronounced lateral growth in the $\langle 1\bar{1}00 \rangle$-directions. This might explain the oddly shaped, but purely m-plane nanorods depicted in the top image of Fig. 5.

In the case of a- and m-plane NFs, their main distinctions are the different top facet angles, their axial growth rates and the pronounced shoulder at the a-plane NF ends compared to their m-plane counterparts. The different top facet angles might origin from the fact that in each facet family (either $\{1\bar{1}0n\}$ or $\{11\bar{2}n\}$, respectively) the most stable facets evolve, which might not have necessarily the same n-value (angle). However, for the $\{1\bar{1}0n\}$-family top facets, which we find in the case of a-/m-plane NWs and m-plane NFs, we always observe $n = 2$, which matches the equilibrium crystal shape calculations by Li *et al.*[30] Nevertheless, NWs grown at higher N fluxes also expose facets with $n > 2$. Due to their higher growth rate, the equilibrium crystal shape may not form. Instead, their rounded NW top facets are the result of a different equilibrium growth shape that occurs under impinging Ga and N fluxes.

The increased axial growth rate of a-plane NFs and the occurrence of a shoulder at their fin tails can be explained by the Ga diffusion kinetics at the non-polar facets: From density-functional theory calculations, it is known that there exists a large anisotropy in the preferred Ga diffusion direction: While the Ga adatoms on the m-plane diffuse mainly in the lateral direction perpendicular to [0001], the atoms on a-plane surfaces have higher diffusion lengths parallel to the c axis.[33] The observed NF dimensions are a direct consequence of these kinetics, as the pronounced lateral diffusion on the m-plane fins triggers lateral growth resulting in thicker NFs while the preferred axial diffusion on the a-plane results in higher, thinner NFs. Further, for both kinds of NFs m-plane tails evolve, as it is not possible to force a certain plane on their end facets by defining their orientation relative to the substrate. In the case of an m-plane NF, no difference to the rest of the fin occurs there. In contrast, in Fig. 7(c), we observe a junction between the a-plane NF and its m-plane end facets. Due to the anisotropic Ga diffusion kinetics, a thicker, but shorter NF end evolves compared to the rest of the NF. Consequently, this reduced NF end height matches exactly the level of the NWs and the m-plane NFs. Finally, this observed anisotropy of the Ga diffusion confirms the proposed NW formation mechanisms. If the a-plane NWs would have exposed a-plane facets throughout the whole growth process, they should be significantly higher than the m-plane NWs. In contrast, their "m-plane past life" explains their lower height. Nevertheless, the a-plane facets, which are forming afterwards at the NW bottom might accelerate the filling of the star gaps at the upper NW parts aiding their mainly hexagonal, a-plane shape.

E. Side facet tuning of GaN nanowires

Figure 8 shows how the side facets of GaN NWs can be tuned as a function of the III–V ratio. Here, we distinguish between the Ga- and the N-limited growth regimes (illustrated by the purple line). We can switch from the N-limited to the Ga-limited regime by e.g., lowering the Ga flux during MBE (cf. Ga flux series in Sec. II B). In the Ga-limited regime, we obtain m-plane NWs. In the N-limited growth regime, the side facets can be controlled by the III–V ratio: At high III–V ratios, we achieve well-shaped m-plane NWs. In contrast, we observe a-plane NWs when a low III–V ratio

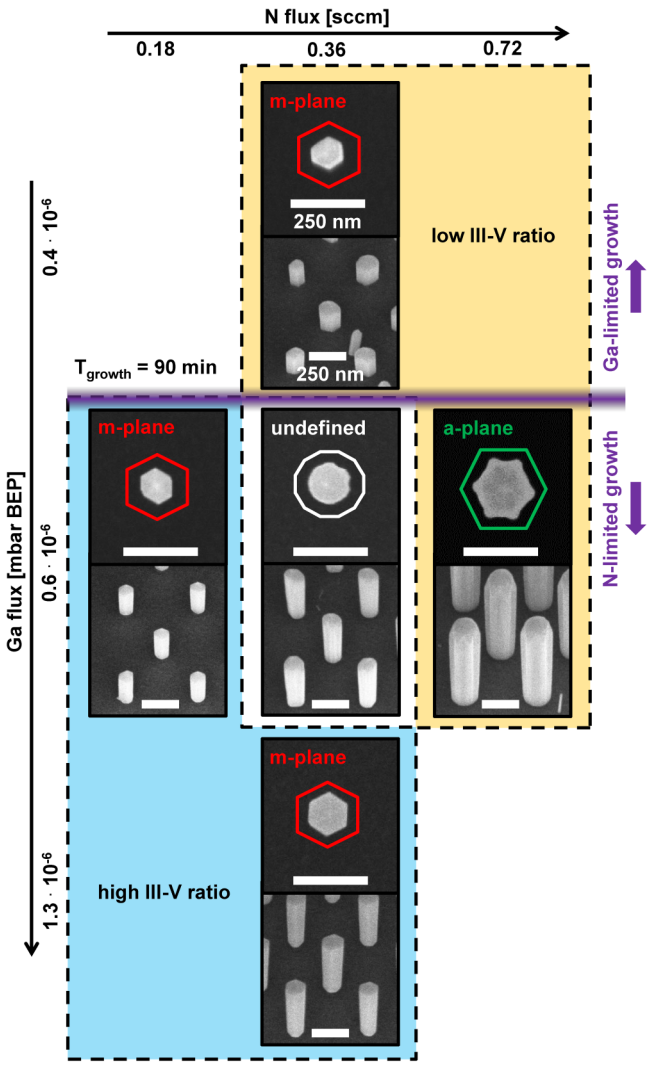

FIG. 8. Top and 45°-tilted view SEM images showing the side facet tuning of GaN nanowires in dependence of the III-V ratio. The N flux is increased from the left to the right and the Ga flux is increased from the top to the bottom. The purple line marks the transition from the Ga- to the N-limited growth regime. The white scale bars mark a distance of 250 nm.

was used during MBE growth. In the intermediate regime with a medium III–V ratio, no clearly defined side facets were achieved. In summary, the NWs tend to have m-plane side facets, whereas a-plane NWs were only observed for low III–V ratios in the N-limited growth regime.

F. Photoluminescence properties

Low temperature PL measurements were performed in order to analyze the structural and electronic properties of ensembles of NSs. Figure 9 shows the PL spectra of GaN NWs as well as a- and

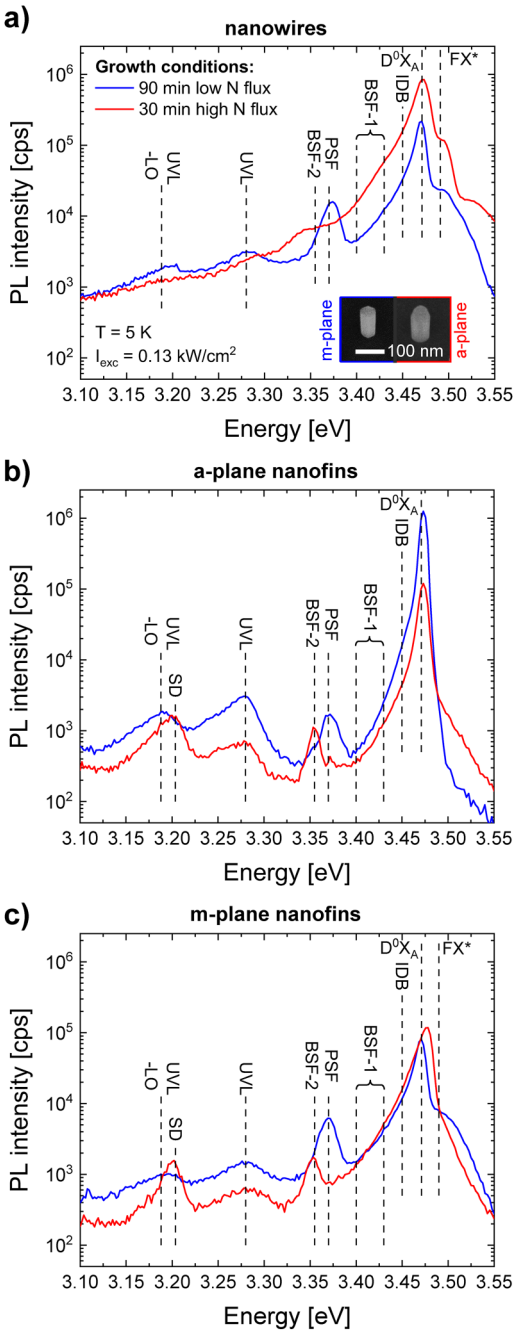

FIG. 9. Low temperature (5 K) PL spectra of the near-band edge region of GaN (a) NWs, (b) a-plane NFs and (c) m-plane NFs grown for 90 min (30 min) with a N flux of 0.18 SCCM (0.73 SCCM) depicted in blue (red). The black dashed lines mark the emission energies attributed to the ultraviolet luminescence (UVL) with their LO phonon replica, an exciton bound to a structural defect (SD), basal plane stacking faults of type I and II (BSF-1/2), prismatic stacking faults (PSF), polarity inversion domain boundaries (IDB), the donor-bound exciton recombination into the A-valence band (D^0X_A) and the proposed free exciton (FX*).

m-plane NFs at 5 K. Each of these three spectra depicts the PL properties of GaN NSs either grown for 90 min at 0.18 SCCM (blue graphs) or for 30 min at 0.73 SCCM (red) in order to compare NSs with similar heights of approx. 200 nm and thicknesses between 100 and 135 nm. An emission at energies of approx. 3.28 eV with LO phonon replica at lower energies shifted by 92 meV can be identified especially for the NSs grown at low N fluxes. This feature is characteristic for the so-called ultraviolet luminescence (UVL) and is attributed to transitions to shallow acceptors from either shallow donors (donor–acceptor-pair, DAP) or from free electrons (conduction-band-acceptor, e-A).[34] For NSs grown at a high N flux, this feature is less pronounced and even barely visible in the case of the NWs. The LO phonon UVL-feature should not be mixed up with the 3.20 eV emission, which might be attributed to an exciton bound to a structural defect (SD).[34] We can observe a pronounced emission of this defect only for the NFs grown at high N fluxes. Interestingly, the occurrence of this SD emission strongly correlates with an emission at 3.35 eV, which is in accordance to c-plane GaN epi-layers in the literature,[34–36] but is in contrast to selective GaN NWs on diamond[37] and epitaxial m-plane GaN.[38] In our study, we observe this 3.35 eV feature only for NSs grown under high N fluxes, especially in the case of the NFs. It might be attributed to basal plane stacking faults of type II (BSF-2) with a stacking sequence of ABABCAC, as observed in m-plane GaN layers grown by MBE.[38] The higher amount of BSF-2 in the high N flux GaN NSs might arise from their significantly higher axial growth rate compared to NSs grown at lower N fluxes [cf. Fig. 4(a)]. At a slightly higher energy of 3.37 eV, we observe a peak which was only detected from the low N flux NSs. We exclude that this transition is just a shifted BSF-2 luminescence, as we have no correlation with the SD emission. Further, BSFs are ideal phase quantum wells, which are influenced by their size, polarization fields, and strain.[39,40] A blue-shift would either point to a smaller lateral extension of the quantum wells, which seems improbably as we always observe a shift of exactly 20 meV, regardless of the kind of NS. On the other hand, the blue-shift could result from compressive strain, which we exclude as the stacking fault peaks would be expected to be broadened and, further, as the donor-bound exciton *via* the A valence band (D^0X_A) luminescence energy is the same for both N fluxes. In the literature, a 3.37 eV luminescence can be attributed to prismatic stacking faults (PSF) in the non-polar direction, in particular, in the m-plane direction.[41] This fits the growth morphology of our low N flux NSs, as we observe a steady lateral growth of the m-plane NWs and NFs as discussed above. Moreover, also the a-plane NFs might evolve from several nucleation spots, which coalescence in the m-plane directions during MBE growth, causing PSFs. Independently of the N flux, we see a broadening of the main emission in the region where we expect basal plane stacking faults of type I (BSF-1) (3.40–3.43 eV), which differ from the type II BSFs due to their altered stacking sequence of ABABCBC.[42,43] Further, we only slightly observe a luminescence at 3.45 eV attributed to polarity inversion domain boundaries (IDB).[44,45] Although there should not be N-polar GaN nuclei on Al-polar AlN substrates at all, even homoepitaxially grown GaN NWs are known to be able to form IDBs, which can be caused by impurities at the interface between the wires and the substrate arising from contaminations during the nano-fabrication process.[46] The most pronounced emission at 3.47 eV arises from the donor-bound excitons D^0X_A. Note that in the case of m-plane NFs grown at a high N flux, this luminescence is slightly shifted toward higher energies by 5 meV, which might be due to residual compressive strain arising from the lattice mismatch with the AlN substrate. Interestingly, both NW samples as well as the m-plane NFs grown at a low N flux show a high energy shoulder at approx. 3.49 eV, which might be attributed to the emission of free excitons (FX*) even though the energetic distance between D^0X_A and FX* is too large (20 meV instead of 7 meV[47]). Note that the attribution of the various defect luminescence lines discussed above is based on the literature. In order to classify the quality of the nanostructures, the PL spectra of the a-plane NFs are shown in the Supporting Information in comparison with those of commercial GaN substrates. A more detailed analysis as well as an extended study of the shifted FX* emission will be provided in a future publication.

IV. CONCLUSION

The present study shows the influence of the III–V ratio during molecular beam epitaxy (MBE) on the formation and nature of the crystal side facets of GaN nanostructures (NSs). In particular, we demonstrate the selective growth of m- and a-plane nanowires (NWs) by determining the N flux during growth. Additionally, the Ga flux enables the adjustment of the exposed non-polar side facets. A growth time variation study shows the cross-sectional evolution of the NWs. Our proposed NW formation mechanism suggests the volume growth rate being responsible for the exposure of the different side facets: While at low N fluxes thin NWs are able to form complete hexagonal m-plane cross sections, there exists a relative Ga shortage for thicker NWs and those grown at higher N fluxes. This leads to a star-like m-plane cross section, which fills up to an a-plane hexagon in the further growth process. Regarding the nanofins (NFs), we can explain the higher a-plane NFs with a pronounced flank at the fin ends by anisotropy in the Ga diffusion kinetics and, thus, can experimentally support the theoretical prediction on this issue. A photoluminescence (PL) study reveals that the main emission is due to donor-bound excitons and it shows that the nature of stacking faults depends on whether the NS growth was conducted under low or high N fluxes.

SUPPLEMENTARY MATERIAL

See the supplementary material for atomic force microscopy images of the AlN substrates, x-ray diffraction data, and scanning electron microscopy images of GaN nanofins grown at different N fluxes.

ACKNOWLEDGMENTS

This work was funded by the Deutsche Forschungsgemeinschaft (DFG, German Research Foundation) under Germany's Excellence Strategy—EXC 2089/1—390776260. Supported by Deutsche Forschungsgemeinschaft (DFG) through TUM International Graduate School of Science and Engineering (IGSSE), GSC 81. The authors thank C. Paulus for the great support in the laboratories.

AUTHOR DECLARATIONS

Conflict of Interest

The authors have no conflicts to disclose.

Author Contributions

Florian Pantle: Conceptualization (lead); Investigation (equal); Writing – original draft (lead); Writing – review & editing (lead). **Monika Karlinger:** Investigation (equal). **Simon Wörle:** Investigation (equal). **Fabian Becker:** Investigation (equal). **Theresa Höldrich:** Investigation (equal). **Elise Sirotti:** Investigation (equal). **Max Kraut:** Investigation (equal). **Martin Stutzmann:** Supervision (lead).

DATA AVAILABILITY

The data that support the findings of this study are available within the article and its supplementary material.

REFERENCES

[1]R. Koester, D. Sager, W.-A. Quitsch, O. Pfingsten, A. Poloczek, S. Blumenthal, G. Keller, W. Prost, G. Bacher, and F.-J. Tegude, "High-speed GaN/GaInN nanowire array light-emitting diode on silicon (111)," Nano Lett. **15**, 2318–2323 (2015).

[2]B. O. Jung, S.-Y. Bae, S. Lee, S. Y. Kim, J. Y. Lee, Y. Honda, and H. Amano, "Emission characteristics of InGaN/GaN core-shell nanorods embedded in a 3D light-emitting diode," Nanoscale Res. Lett. **11**, 1–10 (2016).

[3]M. Philip, D. Choudhary, M. Djavid, K. Le, J. Piao, and H. Nguyen, "High efficiency green/yellow and red InGaN/AlGaN nanowire light-emitting diodes grown by molecular beam epitaxy," J. Sci.: Adv. Mater. Devices **2**, 150–155 (2017).

[4]X. Dai, A. Messanvi, H. Zhang, C. Durand, J. Eymery, C. Bougerol, F. H. Julien, and M. Tchernycheva, "Flexible light-emitting diodes based on vertical nitride nanowires," Nano Lett. **15**, 6958–6964 (2015).

[5]N. Sone, A. Suzuki, H. Murakami, N. Goto, M. Terazawa, W. Lu, D.-P. Han, K. Iida, M. Ohya, M. Iwaya, T. Takeuchi, S. Kamiyama, and I. Akasaki, "Improved uniform current injection into core-shell-type GaInN nanowire light-emitting diodes by optimizing growth condition and indium-tin-oxide deposition," Phys. Status Solidi A **217**, 1900715 (2020).

[6]M. Nami, A. Rashidi, M. Monavarian, S. Mishkat-Ul-Masabih, A. K. Rishinaramangalam, S. R. Brueck, and D. Feezell, "Electrically injected GHz-class GaN/InGaN core-shell nanowire-based μLEDs: Carrier dynamics and nanoscale homogeneity," ACS Photonics **6**, 1618–1625 (2019).

[7]H. Q. T. Bui, R. T. Velpula, B. Jain, O. H. Aref, H.-D. Nguyen, T. R. Lenka, and H. P. T. Nguyen, "Full-color InGaN/AlGaN nanowire micro light-emitting diodes grown by molecular beam epitaxy: A promising candidate for next generation micro displays," Micromachines **10**, 492 (2019).

[8]M. F. Fatahilah, K. Strempel, F. Yu, S. Vodapally, A. Waag, and H. S. Wasisto, "3D GaN nanoarchitecture for field-effect transistors," Micro Nano Eng. **3**, 59–81 (2019).

[9]K. Strempel, F. Römer, F. Yu, M. Meneghini, A. Bakin, H.-H. Wehmann, B. Witzigmann, and A. Waag, "Vertical 3D gallium nitride field-effect transistors based on fin structures with inverted p-doped channel," Semicond. Sci. Technol. **36**, 014002 (2021).

[10]C.-T. Lee and J.-C. Guo, "Fin-gated nanochannel array gate-recessed AlGaN/GaN metal-oxide-semiconductor high-electron-mobility transistors," IEEE Trans. Electron Devices **67**, 1939–1945 (2020).

[11]K.-S. Im, S. J. An, C. G. Theodorou, G. Ghibaudo, S. Cristoloveanu, and J.-H. Lee, "Effect of gate structure on the trapping behavior of GaN junctionless FinFETs," IEEE Electron Device Lett. **41**, 832–835 (2020).

[12]M. Wu, X.-H. Ma, L. Yang, M. Zhang, Q. Zhu, X.-C. Zhang, B. Hou, X.-F. Zheng, and Y. Hao, "Investigation of the nanochannel geometry modulation on self-heating in AlGaN/GaN Fin-HEMTs on Si," Appl. Phys. Lett. **115**, 083505 (2019).

[13]G. Doundoulakis, A. Adikimenakis, A. Stavrinidis, K. Tsagaraki, M. Androulidaki, F. Iacovella, G. Deligeorgis, G. Konstantinidis, and A. Georgakilas, "Nanofabrication of normally-off GaN vertical nanowire MESFETs," Nanotechnology **30**, 285304 (2019).

[14]J. Kamimura, P. Bogdanoff, J. Laehnemann, C. Hauswald, L. Geelhaar, S. Fiechter, and H. Riechert, "Photoelectrochemical properties of In, (In, Ga)N nanowires for water splitting investigated by *in situ* electrochemical mass spectroscopy," J. Am. Chem. Soc. **135**, 10242–10245 (2013).

[15]P. Varadhan, H.-C. Fu, D. Priante, J. R. D. Retamal, C. Zhao, M. Ebaid, T. K. Ng, I. Ajia, S. Mitra, I. S. Roqan *et al.*, "Surface passivation of GaN nanowires for enhanced photoelectrochemical water-splitting," Nano Lett. **17**, 1520–1528 (2017).

[16]L. Zhang, Y. Li, X. Xiu, G. Xin, Z. Xie, T. Tao, B. Liu, P. Chen, R. Zhang, and Y. Zheng, "Preparation of vertically aligned GaN@Ga_2O_3 core-shell heterostructured nanowire arrays and their photocatalytic activity for degradation of Rhodamine B," Superlattices Microstruct. **143**, 106556 (2020).

[17]R. Calarco, T. Stoica, O. Brandt, and L. Geelhaar, "Surface-induced effects in GaN nanowires," J. Mater. Res. **26**, 2157 (2011).

[18]J. Teubert, P. Becker, F. Furtmayr, and M. Eickhoff, "GaN nanodiscs embedded in nanowires as optochemical transducers," Nanotechnology **22**, 275505 (2011).

[19]K. Maier, A. Helwig, G. Müller, J. Schörmann, and M. Eickhoff, "Photoluminescence detection of surface oxidation processes on InGaN/GaN nanowire arrays," ACS Sens. **3**, 2254–2260 (2018).

[20]M. Kraut, F. Pantle, S. Wörle, E. Sirotti, A. Zeidler, F. Eckmann, and M. Stutzmann, "Influence of environmental conditions and surface treatments on the photoluminescence properties of GaN nanowires and nanofins," Nanotechnology **32**, 495703 (2021).

[21]M. Kraut, F. Pantle, J. Winnerl, M. Hetzl, F. Eckmann, I. D. Sharp, and M. Stutzmann, "Photo-induced selective etching of GaN nanowires in water," Nanoscale **11**, 7967–7975 (2019).

[22]R. Volkov, N. I. Borgardt, O. V. Konovalov, S. Fernández-Garrido, O. Brandt, and V. M. Kaganer, "Cross-sectional shape evolution of GaN nanowires during molecular beam epitaxy growth on Si (111)," Nanoscale Adv. **4**, 562–572 (2022).

[23]J. Winnerl, M. Kraut, S. Artmeier, and M. Stutzmann, "Selectively grown GaN nanowalls and nanogrids for photocatalysis: Growth and optical properties," Nanoscale **11**, 4578–4584 (2019).

[24]Z. Gacevic, D. Gomez Sanchez, and E. Calleja, "Formation mechanisms of GaN nanowires grown by selective area growth homoepitaxy," Nano Lett. **15**, 1117–1121 (2015).

[25]P. Ciechanowicz, S. Gorantla, P. P. Michałowski, E. Zdanowicz, J.-G. Rousset, D. Hlushchenko, K. Adamczyk, D. Majchrzak, R. Kudrawiec, and D. Hommel, "Arsenic-induced growth of dodecagonal GaN microrods with stable a-plane walls," Adv. Opt. Mater. **9**, 2001348 (2021).

[26]M. Hetzl, M. Kraut, T. Hoffmann, and M. Stutzmann, "Polarity control of heteroepitaxial GaN nanowires on diamond," Nano Lett. **17**, 3582–3590 (2017).

[27]F. Schuster, M. Hetzl, S. Weiszer, J. A. Garrido, M. De La Mata, C. Magen, J. Arbiol, and M. Stutzmann, "Position-controlled growth of GaN nanowires and nanotubes on diamond by molecular beam epitaxy," Nano Lett. **15**, 1773–1779 (2015).

[28]M. Hetzl, F. Schuster, A. Winnerl, S. Weiszer, and M. Stutzmann, "Reprint of: GaN nanowires on diamond," Mater. Sci. Semicond. Process. **55**, 32–45 (2016).

[29]M. Gruart, G. Jacopin, and B. Daudin, "Role of Ga surface diffusion in the elongation mechanism and optical properties of catalyst-free GaN nanowires grown by molecular beam epitaxy," Nano Lett. **19**, 4250–4256 (2019).

[30]H. Li, L. Geelhaar, H. Riechert, and C. Draxl, "Computing equilibrium shapes of wurtzite crystals: The example of GaN," Phys. Rev. Lett. **115**, 085503 (2015).

[31]C. Blumberg, F. Wefers, F.-J. Tegude, N. Weimann, and W. Prost, "Mask-less MOVPE of arrayed n-GaN nanowires on site-and polarity-controlled AlN/Si templates," CrystEngComm **21**, 7476–7488 (2019).

[32]S. Fernández-Garrido, V. M. Kaganer, K. K. Sabelfeld, T. Gotschke, J. Grandal, E. Calleja, L. Geelhaar, and O. Brandt, "Self-regulated radius of spontaneously formed GaN nanowires in molecular beam epitaxy," Nano Lett. **13**, 3274–3280 (2013).
[33]L. Lymperakis and J. Neugebauer, "Large anisotropic adatom kinetics on nonpolar GaN surfaces: Consequences for surface morphologies and nanowire growth," Phys. Rev. B **79**, 241308 (2009).
[34]M. A. Reshchikov and H. Morkoç, "Luminescence properties of defects in GaN," J. Appl. Phys. **97**, 5–19 (2005).
[35]M. A. Reshchikov, D. Huang, F. Yun, P. Visconti, L. He, H. Morkoç, J. Jasinski, Z. Liliental-Weber, R. J. Molnar, S. S. Park, and K. Y. Lee, "Unusual luminescence lines in GaN," J. Appl. Phys. **94**, 5623–5632 (2003).
[36]M. Reshchikov, D. Huang, L. He, H. Morkoç, J. Jasinski, Z. Liliental-Weber, S. Park, and K. Lee, "Manifestation of edge dislocations in photoluminescence of GaN," Physica B **367**, 35–39 (2005).
[37]F. Pantle, F. Becker, M. Kraut, S. Wörle, T. Hoffmann, S. Artmeier, and M. Stutzmann, "Selective area growth of GaN nanowires and nanofins by molecular beam epitaxy on heteroepitaxial diamond (001) substrates," Nanoscale Adv. **3**, 3835–3845 (2021).
[38]Y. J. Sun, O. Brandt, U. Jahn, T. Y. Liu, A. Trampert, S. Cronenberg, S. Dhar, and K. H. Ploog, "Impact of nucleation conditions on the structural and optical properties of m-plane GaN (1−100) grown on $\gamma - LiAlO_2$," J. Appl. Phys. **92**, 5714–5719 (2002).
[39]G. Jacopin, L. Rigutti, L. Largeau, F. Fortuna, F. Furtmayr, F. Julien, M. Eickhoff, and M. Tchernycheva, "Optical properties of wurtzite/zinc-blende heterostructures in GaN nanowires," J. Appl. Phys. **110**, 064313 (2011).
[40]C. Stampfl and C. G. Van de Walle, "Energetics and electronic structure of stacking faults in AlN, GaN, and InN," Phys. Rev. B **57**, R15052 (1998).
[41]S. Khromov, B. Monemar, V. Avrutin, H. Morkoç, L. Hultman, and G. Pozina, "Correlation between Si doping and stacking fault related luminescence in homoepitaxial m-plane GaN," Appl. Phys. Lett. **103**, 192101 (2013).
[42]R. Liu, A. Bell, F. Ponce, C. Chen, J. Yang, and M. A. Khan, "Luminescence from stacking faults in gallium nitride," Appl. Phys. Lett. **86**, 021908 (2005).
[43]A. Urban, M. Müller, C. Karbaum, G. Schmidt, P. Veit, J. Malindretos, F. Bertram, J. Christen, and A. Rizzi, "Optical emission of individual GaN nanocolumns analyzed with high spatial resolution," Nano Lett. **15**, 5105–5109 (2015).
[44]P. Aseev, Ž. Gačević, A. Torres-Pardo, J. González-Calbet, and E. Calleja, "Improving optical performance of GaN nanowires grown by selective area growth homoepitaxy: Influence of substrate and nanowire dimensions," Appl. Phys. Lett. **108**, 253109 (2016).
[45]T. Auzelle, B. Haas, M. Den Hertog, J.-L. Rouvière, B. Daudin, and B. Gayral, "Attribution of the 3.45 eV GaN nanowires luminescence to inversion domain boundaries," Appl. Phys. Lett. **107**, 051904 (2015).
[46]P. Blanchard, M. Brubaker, T. Harvey, A. Roshko, N. Sanford, J. Weber, and K. A. Bertness, "Characterization of sub-monolayer contaminants at the regrowth interface in GaN nanowires grown by selective-area molecular beam epitaxy," Crystals **8**, 178 (2018).
[47]D. Volm, K. Oettinger, T. Streibl, D. Kovalev, M. Ben-Chorin, J. Diener, B. K. Meyer, J. Majewski, L. Eckey, A. Hoffmann, H. Amano, I. Akasaki, K. Hiramatsu, and T. Detchprohm, "Exciton fine structure in undoped GaN epitaxial films," Phys. Rev. B **53**, 16543 (1996).